

Optical filter with very large stopband (≈ 300 nm) based on a photonic-crystal vertical-directional coupler

M. Grande,^{1,2,*} L. O'Faolain,¹ T. P. White,¹ M. Spurny,¹ A. D'Orazio,² and T. F. Krauss¹

¹*School of Physics and Astronomy, University of St Andrews, St Andrews, Fife, KY169SS, UK*

²*Dipartimento di Elettrotecnica ed Elettronica, Politecnico di Bari, Via Re David 200, 70125, Bari, Italy*

*Corresponding author: grande@deemail.poliba.it

Received July 9, 2009; revised September 21, 2009; accepted September 22, 2009;
posted October 1, 2009 (Doc. ID 113407); published October 23, 2009

We have designed, fabricated, and demonstrated a vertical directional coupler based on the coupling between a polymer waveguide and a W1 photonic crystal waveguide. The filters have a bandwidth of ~ 2 nm within a stopband of $\Delta\lambda \approx 300$ nm and an on-chip insertion loss of 1 dB. This is the first (to our knowledge) demonstration of a filter with such a large stopband that overcomes the bandwidth limitation of existing filters. © 2009 Optical Society of America

OCIS codes: 230.5298, 130.7408.

Optical filters are key building blocks for wavelength-division-multiplexing applications. A number of schemes are currently used to realize this multiplexing function, such as arrayed waveguide gratings, microring resonators [1,2], and coupled-ring resonator systems [3,4]. Most of these fall short when a large free spectral range (FSR) is required, as, for example, in the combined L-C optical telecommunication bands ($\Delta\lambda \sim 100$ nm), in multimodal biosensing, or in astrophotonics applications. A widely used filter is the microring resonator, with the highest FSR of 47 nm reported to date, using a ring radius of $2 \mu\text{m}$ [1], or even >60 nm based on the Vernier effect [2]. The FSR is limited by the size of the microring, however, and bending losses would increase sharply if the device were made even smaller to achieve a higher FSR.

As photonic crystals (PhCs) typically exhibit a very wide bandgap (300–400 nm), they have potential as the basis for wide-stopband filters. Filters based on the popular L3 PhC cavity have been proposed, but these suffer from a relatively low (tens of nanometers) FSR [5] owing to the multimodal nature of the cavity. Heterostructure PhC cavities [6] are limited to a similar range owing to the proximity of the waveguide mode. Evanescent mode coupling [7] and attenuated total reflection [8] suggest an alternative approach. In these cases, filtering occurs only when the propagation constants of the respective modes

are matched, leaving the stopband uncompromised.

Based on this concept, we design and demonstrate a slow-light PhC waveguide combined with a polymer waveguide as a directional-coupler-based filter (Fig. 1) with a very large stopband. It should be noted that the bandwidth-limiting parameter here is the stopband of the PhC rather than the FSR of the filter, as in other configurations. As discussed in [9], the spectral position of the PhC waveguide within the stopband depends only on its width, so the filter response can be placed anywhere within this range. The advantage of the 2D PhC approach compared to a 1D realization is that the width of the stopband and the coupling length of the grating can be optimized almost independently.

In a two-waveguide coupled system, coupling occurs when the two propagation constants coincide [10–12]. From an analytical point of view, the coupled bandwidth $\Delta\lambda$ is given by [13]

$$\Delta\lambda = \frac{2\lambda_0^2\kappa}{\pi\left(\frac{\partial\beta_1}{\partial\omega} - \frac{\partial\beta_2}{\partial\omega}\right)} = \frac{2\lambda_0^2\kappa}{\pi(n_{g1} - n_{g2})}, \quad (1)$$

where λ_0 , κ , β_i , n_{gi} ($i=1,2$), are the coupling wavelength, the coupling coefficient, the propagation constants, and the group index, respectively. Equation (1) shows that in order to achieve a narrow band-

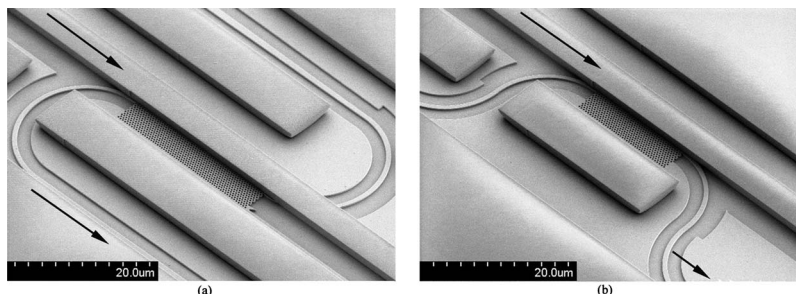


Fig. 1. Micrograph of the fabricated devices without an intermediate oxide layer (the arrangement on the left is used to monitor the counterpropagating mode, while on the right, we monitor the copropagating mode. The flow of light is from top left to bottom right in each case, as indicated by the arrows).

width, a large-group-index difference and a small coupling coefficient κ are required. On the other hand, κ is related to the coupling efficiency at the drop port by

$$T(L) = \tanh^2(\kappa L), \quad (2)$$

where T and L are the transmission at the output port and the length of the device, respectively. Equation (2) shows the importance of finding a trade-off between the coupling coefficient κ and the length of the device. Figure 2(a) depicts the dispersion curve of the W1 PhC waveguide superimposed onto that of a polymer ridge waveguide. These two curves refer to the TE polarization and have been created using the plane-wave expansion method with refractive indices of 3.48, 1.54, and 1.4 for the silicon layer, the polymer waveguide, and the silica layer, respectively. It is worthwhile pointing out that the two waveguides have very different group velocities, as indicated by the different slopes in the band diagram. This dissimilarity creates an anticrossing between the two dispersion curves and gives rise to a ministopband [Fig. 2(b)]. The coupling coefficient at the intersection point is related to the spectral width of the anticrossing. Figure 2(b) also shows the supermodes of the vertical coupler. The ministopband forces the input signal to be coupled into a backward-propagating mode, so the two supermodes are counterpropagating in this case. Furthermore, Fig. 2(a) also shows that the dispersion curve of the polymer waveguide intersects the odd mode of the PhC waveguide. The coupling between these two modes is negligible because of symmetry, so coupling to the odd mode does not limit the operating range. The TM mode of the low-index waveguide can also couple to the TM mode of the W1 waveguide. This occurs at a different wavelength to than that for the TE modes. For a filter, this is undesirable and limits the operation of this device to the TE polarization.

We fabricated the device from a SOITEC silicon-on-insulator wafer comprising a nominally 220-nm-thick silicon layer on 2 μm of silica [14]. The PhC was fabricated by means of e-beam lithography, using ZEP-520A as a positive resist. The structure was transferred into the substrate by means of a dry-etching process in a reactive-ion-etching system using CHF_3 and SF_6 as described elsewhere [15,16]. The sample was then covered by a layer of FOx14 (Flowable Oxide) from Dow Corning by spin coating after the re-

sist removal. The FOx penetrates the holes of the photonic crystal, as demonstrated in [16]. This layer is then annealed at 500°C for 1 h in N_2 atmosphere [17]. The polymer waveguide is created by using two layers of ZEP for a total thickness of about 2 μm , and a second e-beam lithography step (the fabricated cross section is 2 $\mu\text{m} \times 4 \mu\text{m}$). To verify the theoretical assumptions, we fabricated two different types of devices, which allows us to measure the counter-propagating and the forward-propagating signals. In both cases, a set of photonic wires are used to collect the light from the PhC waveguide. The specific layout of the respective waveguides was chosen to avoid a coupling of light from the polymer waveguide directly into the access waveguides or into the substrate. Furthermore, in order to enable coupling between the “fast-light” wire waveguide and the “slow-light” PhC waveguide, we have incorporated an interface region consisting of 10 rows of holes with slightly increased (30 nm) lattice constant in the propagation direction [18].

A supercontinuum source (Koheras Super-K Compact) was used to characterize the devices in the wavelength range from 1300 nm to 1650 nm for TE polarization. The fabricated devices were realized with and without the FOx layer and with different lengths to determine the coupling length. Figures 3(a) and 3(b) show the measurements of the two devices with lengths of 40 μm and 60 μm and lattice periods of 420 nm and 410 nm, respectively. Maximum coupling occurs at wavelengths of 1587 nm and 1575 nm, respectively. The polymer waveguide mode also couples to the continuum of modes in the dielectric band (for wavelengths >1625 nm), but the coupling is negligible elsewhere [the small peak at 1440 nm in Fig. 3(b) is due to coupling to the odd (first order) mode of the PhC waveguide]. This is related to a small offset error in the alignment between the two waveguides that breaks the symmetry of the device. The measurements therefore confirm that the useful spectral range over which the filter can be operated extends across the entire stopband of the PhC, i.e., across approximately 300 nm.

The FWHM of the coupled signal is 2.5 nm and 1.9 nm, and the sidelobe suppression ratio (SLSR) is 14 dB and 16 dB for the devices without and with an intermediate silica layer, respectively. The propagation losses in the ZEP waveguide are 3 dB/cm and were measured by Fourier transforming the Fabry-

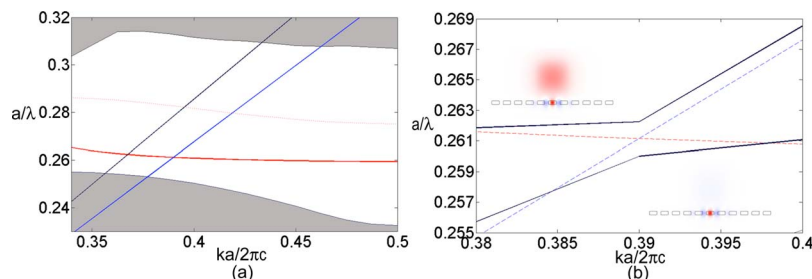


Fig. 2. (Color online) (a) 3-D calculated band structure ($r/a=0.30$): silica lightguide (left vertical curve), 2 $\mu\text{m} \times 2 \mu\text{m}$ cross section polymer waveguide (right vertical curve), W1 waveguide (horizontal curve), odd defect mode (dotted curve), bulk PhC modes (gray); (b): anticrossing point (enlarged) and the even (upper) and odd (lower) supermodes.

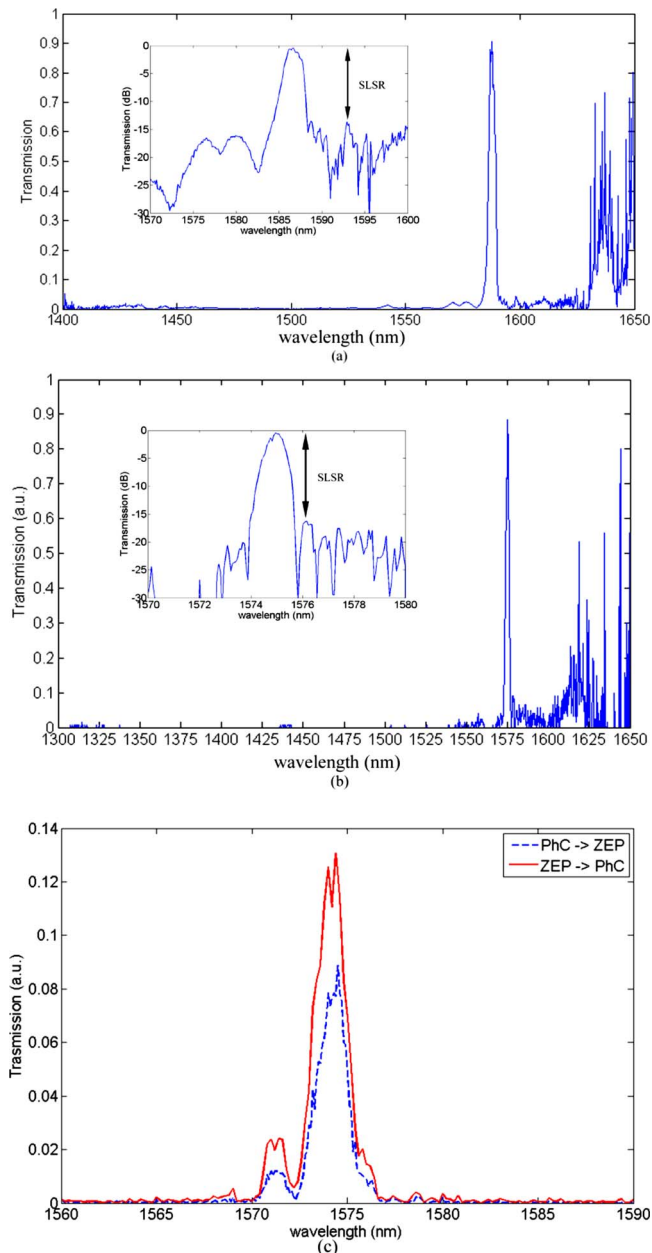


Fig. 3. (Color online) Measured filter response at the drop port (a) without and (b) with the FOx layer (the small peaks at 1310–1325 nm are due to the coupling to the air band). Transmission in (a) is normalized to a straight-through waveguide, and we observe a coupling efficiency $>80\%$ (<1 dB coupling loss); the transmission in (b) and (c) is plotted in arbitrary units. The insets in (a) and (b) show the SLSR. (c) Coupling between the two waveguides launching into the PhC waveguide and into the ZEP waveguide, the sidelobes are related to the sudden onset and termination of coupling between the two waveguides, resulting in a sinclike spectral response.

Perot fringes [19]. The coupling losses (fiber to polymer waveguide) are estimated at 3 dB, and the on-chip insertion loss between the polymer and the PhC waveguide is only about 1 dB, which could be improved further by optimizing the waveguide alignment and coupling length. This low value for the insertion loss is due to the strong coupling between the two waveguides, which at first sight is surprising,

given that the material indices are so different [Fig. 3(c)].

In conclusion, we have demonstrated a new type of slow-light enhanced filter that may be used as the basic element of an on-chip spectrometer with nanometer wavelength resolution. Tailoring the slow-light properties of the PhC waveguides offers the potential for further enhancements in terms of filter response (e.g., achieving a flat-top), sidelobe suppression, as well as tunability, e.g., via localized heating (for applications as a reconfigurable add/drop system). Multiple filters can be cascaded for a multichannel device. The device does not require a spot-size converter, allowing the input signal from an external optical fiber to be coupled directly into the polymer waveguide. The extremely large operating range (~ 300 nm) overcomes the bandwidth limitation of existing filters.

References and Notes

1. M. S. Nawrocka, T. Liu, X. Wang, and R. R. Panepucci, *Appl. Phys. Lett.* **89**, 071110 (2006).
2. B. Timotijevic, G. Mashanovich, A. Michaeli, O. Cohen, V. M. N. Passaro, J. Crnjanski, and G. T. Reed, *Chin. Opt. Lett.* **7**, 56 (2009).
3. S. Xiao, M. H. Khan, H. Shen, and M. Qi, *Opt. Express* **15**, 14765 (2007).
4. M. Popovic, "Theory and design of high-index-contrast microphotonic circuits," Ph.D. thesis (Massachusetts Institute of Technology, 2008).
5. A. R. A. Chalcraft, S. Lam, D. O'Brien, T. F. Krauss, M. Sahin, D. Szymanski, D. Sanvitto, R. Oulton, M. S. Skolnick, A. M. Fox, D. M. Whittaker, H.-Y. Liu, and M. Hopkinson, *Appl. Phys. Lett.* **90**, 241117 (2007).
6. S. Noda, M. Fujita, and T. Asano, *Nature Mater.* **4**, 207 (2005).
7. C. Grillet, C. Smith, D. Freeman, S. Madden, B. Luther-Davies, E. Magi, D. Moss, and B. Eggleton, *Opt. Express* **14**, 1070 (2006).
8. M. Galli, D. Bajoni, M. Patrini, G. Guizzetti, D. Gerace, L. C. Andreani, and M. Belotti, *Phys. Rev. B* **72**, 125322 (2005).
9. H. Benisty, *J. Appl. Phys.* **79**, 7483 (1996).
10. W. Kuang, C. Kim, A. Stapleton, and J. O'Brien, *Opt. Lett.* **27**, 1604 (2002).
11. P. E. Barclay, K. Srinivasan, and O. Painter, *J. Opt. Soc. Am. B* **20**, 2274 (2003).
12. Z. Zhang, U. Andersson, and M. Qiu, *Act. Passive Electron. Compon.* **2007**, doi: 10.1155/2007/78602 (2007).
13. Z. Xu, J. Wang, Q. He, L. Cao, P. Su, and G. Jin, *Opt. Express* **13**, 5608 (2005).
14. The fabrication was carried out in the framework of the ePIXnet Nanostructuring Platform for Photonic Integration; see <http://www.nanophotonics.eu>.
15. L. O'Faolain, X. Yuan, D. McIntyre, S. Thoms, H. Chong, R. M. De la Rue, and T. F. Krauss, *Electron. Lett.* **42**, 1454 (2006).
16. T. P. White, L. O'Faolain, J. Li, L. C. Andreani, and T. F. Krauss, *Opt. Express* **16**, 17076 (2008).
17. M. Haffner, A. Haug, A. Heeren, M. Fleischer, H. Peisert, T. Chassé, and D. P. Kern, *J. Vac. Sci. Technol. B* **25**, 2045 (2007).
18. J. P. Hugonin, P. Lalanne, T. P. White, and T. F. Krauss, *Opt. Lett.* **32**, 2638 (2007).
19. D. Hofstetter and R. Thornton, *Opt. Lett.* **22**, 1831 (1997).